American Mineralogist, Volume 88, pages 481–488, 2003

Electronic structure of Fe-bearing lazulites

M. GRODZICKI,[1,*] G.J. REDHAMMER,[1] G. AMTHAUER,[1] V. SCHÜNEMANN,[2] A.X. TRAUTWEIN,[2] B. VELICKOV,[3] AND P. SCHMID-BEURMANN[4]

[1]Institute of Mineralogy, University of Salzburg, Hellbrunner Str. 34, A-5020 Salzburg, Austria
[2]Institute of Physics, Medical University, Ratzeburger Allee 160, D-23536 Lübeck, Germany
[3]Institute of Applied Geosciences, TU-Berlin, Ernst-Reuter-Platz 1, D-10587 Berlin, Germany
[4]Institute of Mineralogy and Petrography, University of Kiel, Ludewig-Meyn-Str. 10, D-24098 Kiel, Germany

ABSTRACT

The Fe end-members scorzalite [$Fe^{2+}Al_2^{3+}(PO_4)_2(OH)_2$] and barbosalite [$Fe^{2+}Fe_2^{3+}(PO_4)_2(OH)_2$] of the lazulite series have been investigated by Mössbauer and diffuse reflectance spectroscopy, and by electronic structure calculations in the local spin density approximation. The measured quadrupole splitting (ΔE_Q = –3.99 mm/s) in scorzalite is in quantitative agreement with the calculated value (ΔE_Q = –3.90 mm/s), as well as its temperature dependence. The optical spectrum of barbosalite can be resolved into three peaks at 8985 cm^{-1}, 10980 cm^{-1}, and 14110 cm^{-1}. These positions correlate well with the two calculated spin-allowed d-d transitions at 8824 cm^{-1} and 11477 cm^{-1}, and with an intervalence charge transfer transition at about 14200 cm^{-1}. The calculated low-temperature magnetic structure of barbosalite is characterized by a strong antiferromagnetic coupling (J = –84.6 cm^{-1}) within the octahedral Fe^{3+}-chains, whereas a weak antiferromagnetic coupling within the trioctahedral subunit cannot be considered as conclusive. The analysis of the charge and spin densities reveals that more than 90% of the covalent part of the iron-ligand bonds arises from the Fe(4s,4p)-electrons. Clusters of at least 95 atoms are required to reproduce the available experimental data with quantitative accuracy.

INTRODUCTION

The minerals of the lazulite group are basic hydroxo-phosphates with the general chemical composition $M^{2+}M_2^{3+}(PO_4)_2(OH)_2$. They crystallize in the monoclinic space group $P2_1/c$ with two formula units per unit cell (Lindberg and Christ 1959), and comprise, besides the name-giving lazulite with $M^{2+}M_2^{3+}$= $Mg^{2+}Al_2^{3+}$, the end-members scorzalite with $M^{2+}M_2^{3+} = Fe^{2+}Al_2^{3+}$, barbosalite with $M^{2+}M_2^{3+} = Fe^{2+}Fe_2^{3+}$, and hentschelite (Sieber et al. 1987) with $M^{2+}M_2^{3+} = Cu^{2+}Fe_2^{3+}$. A complete solid-solution series has been established between lazulite and scorzalite (Schmid-Beurmann et al. 1999) but not among the other end-members. The crystal structure of lazulite, scorzalite, and barbosalite was first solved correctly by Lindberg and Christ (1959). However, those authors did not refine the atomic coordinates and did not give the the positions of the H-atoms, but that information has been supplied by more-recent structure determinations on lazulite (Giuseppetti and Tadini 1983) and on barbosalite (Redhammer et al. 2000). The structure consists of OH-corner-sharing M^{3+}-octahedra forming chains parallel to the crystallographic **c**-axis. Every second pair of M^{3+}-octahedra of two adjacent chains is linked to each other by an M^{2+}-octahedron along the **b**-axis in such a way that each M^{2+}-octahedron shares faces with two M^{3+}-octahedra. In addition, the M^{3+}-octahedral chains are linked by nearly regular phosphate tetrahedra having one of their pseudo $\bar{4}$-axis oriented along the crystallographic **b**-axis.

Spectroscopic investigations cover studies by optical (Amthauer and Rossman 1984) and Mössbauer spectroscopy (Mattievich et al. 1979; Amthauer and Rossman 1984; Rouzies and Millet 1993; Millet et al. 1995; Schmid-Beurmann et al. 1999; Redhammer et al. 2000). All Mössbauer spectra reveal two distinct doublets corresponding to high-spin Fe^{2+} and Fe^{3+}, respectively. In spite of the rather short Fe-Fe distance of 2.832 Å in barbosalite at room temperature (Redhammer et al. 2000), the Mössbauer spectra up to 400 K do not give any indication for valence delocalization. On the other hand, the dark-green to opaque color suggests the existence of an intervalence transition so that barbosalite belongs to the class 1 of mixed valence compounds (Hush 1967). The low-temperature (80 K) quadrupole splitting of the Fe^{2+} is very large, with 4.04 mm/s in Fe-bearing lazulite (sign not determined, Amthauer and Rossman 1984) and with about –3.80 mm/s in barbosalite (Mattievich et al. 1979; Redhammer et al. 2000) where the negative sign in the latter case has been inferred from the magnetically split spectrum resulting from the magnetic ordering below the Neel temperature of 160 K. This negative sign is unexpected in so far as the first coordination sphere of Fe^{2+} resembles a trigonally elongated octahedron. Consequently, the degeneracy of the t_{2g}-like spin-down orbitals is lifted in such a way that the e_g-like orbitals are below the nondegenerate a_{1g} orbital. Such a splitting pattern, however, should lead to a positive sign for the quadrupole splitting as detected, e.g., in another three-iron cluster with linear arrangement (Paulsen et al. 1994). It is then not clear if the origin of the negative sign of the quadrupole splitting in barbosalite is caused by some specific geometrical arrangement of the higher coordination spheres or by the magnetic interaction of Fe^{2+} with the neighboring Fe^{3+}-ions.

* E-mail: michael.grodzicki@sbg.ac.at

To arrive at a more detailed understanding of the electronic and magnetic structure of the Fe-bearing lazulites, a combined theoretical and experimental study is presented in this work. On the theoretical side, electronic structure calculations were performed in the local spin density approximation (LSDA) on clusters of varying size, geometry, and composition. Experimentally, diffuse reflectance spectra of scorzalite and barbosalite have been recorded that also help to assess the reliability of the theoretical approach. In addition, Mössbauer spectra have been measured in an external field of 7T on scorzalite to explore if the sign of the Fe^{2+} quadrupole doublet remains negative when the neighbouring Fe^{3+}-ions are absent.

Experimental and theoretical methods

Mössbauer spectra on a synthetic scorzalite sample (Schmid-Beurmann et al. 1999) were recorded using a conventional spectrometer in the constant acceleration mode. Isomer shifts are given relative to α-Fe at room temperature. The spectra obtained at low fields (20 mT) were measured in a helium-bath cryostat (Oxford Instruments MD 306) equipped with a pair of circular permanent magnets. For the high-field spectra, a cryostat with a superconducting magnet was used (Oxford Instruments Spectromag 4000). Whereas the low-field spectra were analyzed by least-square fits using Lorentzian line shape without imposing any restrictions, the spectra measured in high magnetic fields were simulated on the basis of the spin-Hamiltonian approximation for paramagnetic Fe centers (Schünemann and Winkler 2000). This procedure includes an averaging over all orientations of the randomly oriented paramagnetic Fe sites as the measurements were performed on powder samples. In order to keep the number of parameters small, the reference frames for the electronic g-tensor, the hyperfine coupling tensor A, and the electric field gradient tensor have been taken as collinear.

The diffuse reflectance spectra of the synthetic scorzalite sample (Schmid-Beurmann et al. 1999) and of a powder sample of the natural barbosalite from Bull Moose Mine, South Dakota U.S.A. (Redhammer et al. 2000), were measured at room temperature on a Perkin-Elmer Lambda 19 spectrometer. A stepscan of 60 nm per minute was used in the range between 30 000 and 5000 cm^{-1} (333 to 2000 nm), and the NIR-sensivity was set on 6. Absorption was measured using the FR-mode based on the Kubelka-Munk relation (Kubelka and Munk 1931; Kortüm and Oelkrug 1966) with teflon as the white reference standard. Because of strong absorption in barbosalite (dark-green color) the sample was diluted with LiF not absorbing in the measured range. Peak positions, half widths, and intensities of the bands were obtained by the PEAKFIT software (Jandel Corporation). The asymmetric baseline caused by Fe^{3+}-O charge-transfer transitions was fitted by the descending part of the function sigmoid, and the line shapes of the absorption bands were assumed to be Gaussians.

The calculations have been performed in local spin density approximation (LSDA) by the spin-polarized, self-consistent charge (SCC-)$X\alpha$ method (Grodzicki 1980, 1985). However, the $X\alpha$-potential (with $\alpha = 0.7$) was only used for the evaluation of the two- and three-center integrals, whereas the one-center integrals are derived from all-electron (relativistic) atomic Dirac-Fock calculations. Furthermore, the core electrons enter the two- and three-center integrals via a pseudopotential also derived from relativistic atomic calculations. The method is hence ab initio in the sense that it does not contain any adjustable parameter. The valence basis set consists of 2s-, 2p-orbitals for O and F; 3s-, 3p-orbitals for Mg, Al, and P; and 3d-, 4s-, 4p-orbitals for Fe.

Within the framework of the LSDA, ionization and excitation energies are usually calculated by the transition-state procedure (Slater 1974). In most cases, this calculation leads to a uniform shift of all orbital energies so that energy differences are affected only to a minor extent. Accordingly, d-d excitation energies are determined as the respective orbital energy differences whereas intervalence charge transfer (IVCT) excitations are computed alternatively as transition-state energies and as total energy differences, respectively. The (isotropic) Heisenberg coupling constant J occurring in the Heisenberg Hamiltonian:

$$H^{AB} = -2J \cdot \vec{S}^A \cdot \vec{S}^B \tag{1}$$

which describes the coupling between two localized spins at sites A and B, is calculated on the basis of the broken symmetry formalism (Noodleman 1981) according to

$$J = -\frac{E(S_{max}) - E(S_{min})}{S^2_{max} - S^2_{min}} \tag{2}$$

where $E(S)$ is the total energy for the spin state S. Positive values of J correspond to parallel or "ferromagnetic", negative values to antiparallel or antiferromagnetic coupling of the two spins $\vec{S}^A$ and $\vec{S}^B$.

The measured quadrupole splitting ΔE_Q is related to the components $|V_{zz}| \geq |V_{yy}| \geq |V_{xx}|$ of the electric field gradient (efg) tensor in its principal axes system by

$$\Delta E_Q = (1/2)\, e_o Q V_{zz}\, (1 + \eta^2 / 3)^{1/2} \tag{3}$$

where e_o denotes the (positive) elementary charge, and the asymmetry parameter $\eta = (V_{xx} - V_{yy})/V_{zz}$, describing the deviation of the efg from axial symmetry, can take values between 0 and 1. The size of the nuclear quadrupole moment Q of the first excited state of ^{57}Fe is assumed to be between 0.15 and 0.17 barn (Ray and Das 1977; Lauer et al. 1979; Dufek et al. 1995; Blaha et al. 2000). Experimentally determined isomer shift differences $\Delta\delta$ of the same Mössbauer nucleus in different chemical environments A and B are related to the corresponding differences of the electron densities $\rho(0)$ at the Mössbauer nuclei:

$$\Delta\delta = \delta_A - \delta_B = \alpha[\rho_A(0) - \rho_B(0)] \tag{4}$$

The isomer shift calibration constant α for ^{57}Fe covers values in the range of $(-0.25 \pm 0.03)\ a_o^3$ mm/s, according to results from nonempirical electronic structure calculations (Duff 1974; Nieuwpoort et al. 1978; Akai et al. 1986; van der Heyden et al.

1987; Zhang et al. 1987; Eriksson and Svane 1989; Jansen et al. 1992).

The calculation of the efg-tensor and of the electron density at the nucleus within the framework of a valence-electron-only electronic structure calculation has been described in detail previously (Grodzicki et al. 1987; Grodzicki and Amthauer 2000). With respect to a basis set of atomic orbitals, the efg tensor can be decomposed into three different contributions, viz., the valence contribution arising from the anisotropy of the valence shell of Fe, the covalence contribution describing the anisotropy of the bonding electrons between Fe and the surrounding ligands, and the ligand contribution arising from the ion cores and the valence electrons of the ligands. The polarization of the core electrons of the Fe atom is accounted for by the Sternheimer shielding function $\gamma(r)$, which has been derived from atomic self-consistent first-order perturbation calculations (Lauer et al. 1979). In the principal axes system of the efg-tensor, the efg V_{zz} is simply the sum of the valence-, covalence-, and ligand-contributions, and the usually dominating valence contribution is roughly proportional to the anisotropies

$$\Delta n_{\mathrm{d}} = n_{x^2-y^2} + n_{xy} - n_{z^2} - (n_{xz} + n_{yz})/2 \quad (5)$$

$$\Delta n_{\mathrm{p}} = (n_x + n_y)/2 - n_z \quad (6)$$

of the Fe(3d)-shell and Fe(4p)-shell occupations n_i of the i-th orbital, respectively. Whereas it follows immediately that the anisotropy of the Fe(3d)-shell dominates the efg for high-spin Fe^{2+}, it is often assumed that for high-spin Fe^{3+} the ligand contribution should be the largest. However, several calculations have demonstrated that the valence contribution generally dominates even when the anisotropy should vanish according to crystal-field theory (Keutel et al. 1999; Grodzicki et al. 2000; Grodzicki et al. 2001).

The central problem in calculating $\rho(0)$ is that, on one side, the amplitudes $\varphi_{is}(0)$ of the s-orbitals at the Mössbauer atom require a very high degree of accuracy whereas on the other side, the core orbitals are not included in a valence-electron-only method. For this reason, the amplitudes $\varphi_{is}(0)$ of both the core and valence s-orbitals at the origin are determined for the free ion by highly accurate, fully numerical (i.e., basis-set free) relativistic atomic calculations for a certain number of valence shell configurations. In case of ^{57}Fe, these configurations are $4s^n\ 3d^m$ with n = 0,1,2 and m = 4,5,6,7 (except for $4s^2\ 3d^7$). From these eleven values, an interpolation formula is derived as a function of the valence shell occupation numbers n_s and n_d for each atomic core and valence s-orbital of Fe:

$$\sqrt{4\pi}\varphi_{\mathrm{i}}^{\mathrm{rel}}(0) = a_{io} + a_{is}n_d + a_{id}n_d + a_{iss}n_s^2 + a_{isd}n_s n_d + a_{idd}n_d^2 \quad (7)$$

It should be emphasized that the valence orbitals of the Mössbauer atom are included in this procedure because the size of the basis set entering the cluster calculation is usually not suffcient, especially for large systems.

Results and discussion I: Scorzalite

The Mössbauer spectra of scorzalite recorded at 4.2 K in fields of (a) 20 mT, (b) 7 T perpendicular, and (c) 7 T parallel to the γ-beam are shown in Figure 1. In the field of 20 mT, a doublet with an isomer shift δ = 1.25 mm/s (relative to α-Fe) and a quadrupole splitting ΔE_Q = 3.99 ± 0.02 mm/s, characteristic for high-spin (S=2) Fe^{2+} is observed. These values are in close agreement with previous low-temperature measurements on an Fe-bearing lazulite (Amthauer and Rossman 1984). The application of large external fields induces a magnetic hyperfine splitting that has been simulated successfully by a spin Hamiltonian formalism (Schünemann and Winkler 2000) with the parameters listed in Table 1. The analysis yields a positive zero field splitting D = 4 cm^{-1} and a nonvanishing rhombicity of E/D = 0.2 ± 0.1. The asymmetry parameter has been determined as $\eta = 0.6 \pm 0.2$, and the sign of the quadrupole splitting

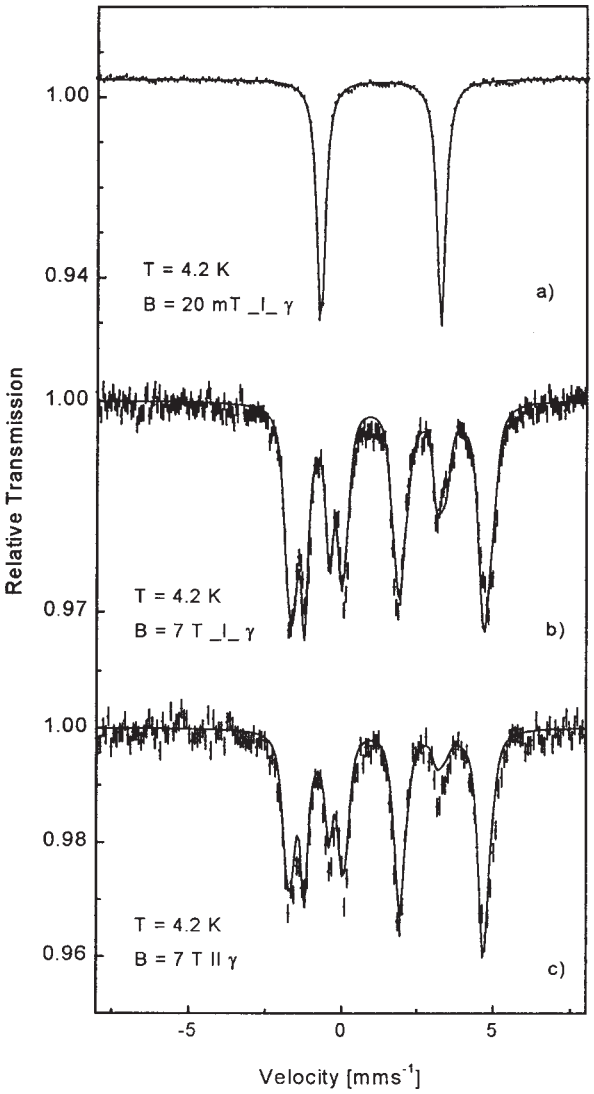

Figure 1. Mössbauer spectra of scorzalite at 4.2 K in fields of (**a**) 20 mT, (**b**) 7 T perpendicular, and (**c**) 7 T parallel to the γ-beam. The solid line in (**a**) is a Lorentzian fit yielding an isomer shift δ = 1.25(2) mm/s, a quadrupole splitting ΔE_Q = 3.99(2) mm/s, and a line width Γ = 0.32(2) mm/s. The solid lines in (**b**) and (**c**) represent spin Hamiltonian simulations with the parameter set of Table 1.

TABLE 1. Hyperfine parameters of high-spin Fe^{2+} (S = 2) in scorzalite for T = 4.2K, as obtained from the spin Hamiltonian simulations *

δ (mm/s)	ΔE_Q (mm/s)	Γ(mm/s)	η	D(cm^{-1})	E/D	$A_{ii}/g_N\mu_N$ (T)
1.25(2)	–3.99(2)	0.27(3)	0.6(2)	4(1)	0.2(1)	–9.7(1.5), –8.4(1.5), –5.4(2.0)

* δ = isomer shift, ΔE_Q = quadrupole splitting, Γ = line width, η = asymmetry parameter, D = zero-field splitting, E/D = rhombicity, A_{ii} = diagonal elements of the hyperfine coupling tensor.

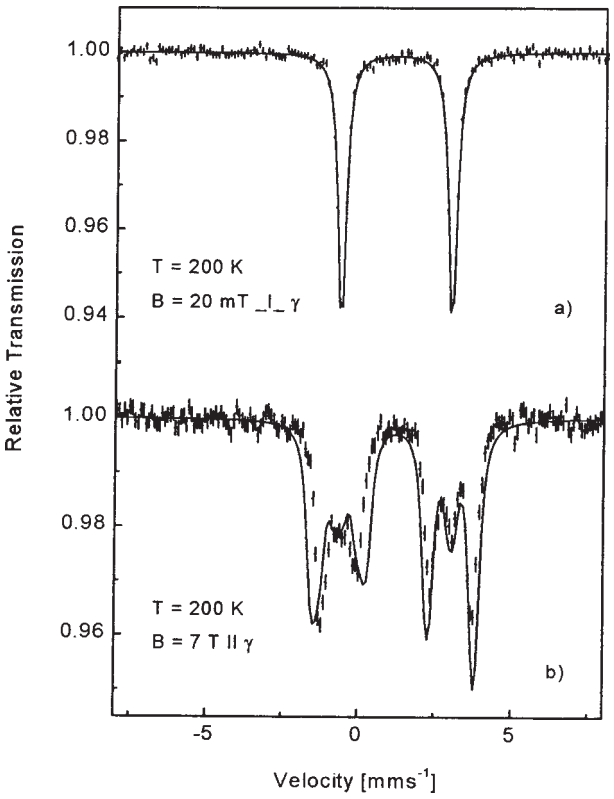

FIGURE 2. Mössbauer spectra of scorzalite at 200 K in fields of (**a**) 20 mT perpendicular and (**b**) 7 T parallel to the γ-beam. The solid line in (**a**) is a Lorentzian fit yielding an isomer shift δ = 1.20(2) mm/s, a quadrupole splitting ΔE_Q = 3.63(2) mm/s, and a line width Γ = 0.32(2) mm/s. The solid line in (**b**) represents a spin Hamiltonian simulation with the parameter set of Table 1, except δ, ΔE_Q, Γ that were taken from the Lorentzian fit of (**a**).

is negative so that the sign of ΔE_Q is invariant with regard to the occupation of the M^{3+}-octahedra with Al or Fe^{3+}, respectively. These results are confirmed by measurements taken at 200 K (Fig. 2). At this temperature, all fine structure levels are equally populated and fast relaxation among them causes a quasidiamagnetic spectrum to be observed. The shape of the spectrum in a field of 7 T (Fig. 2b) again proves the negative sign of the electric field gradient. The spin-Hamiltonian simulation of the spectrum at 200 K with the parameters derived from the field-dependent data at 4.2 K reproduces the asymmetry and the overall shape of the magnetic pattern, but not the details of the magnetic splitting. The misfit between simulated and experimental data may indicate that due to spin-spin interactions, the spins of the Fe sites are not in the fast relaxation limit (i.e., relaxation rate >> $10^7 s^{-1}$) of Mössbauer spectroscopy even at T = 200 K.

The diffuse reflectance spectrum of scorzalite exhibits a broad asymmetric band between 5000 and 20000 cm^{-1} (Fig. 3a), and is almost identical with the optical absorption spectrum of a natural lazulite with 0.19 Fe atoms per formula unit (apfu) (Amthauer and Rossman 1984). At least two absorption lines are necessary to model this broad band; however, the best results are obtained assuming three Gaussian-shaped absorption lines centered at 14870 cm^{-1}, 12120 cm^{-1}, and 10490 cm^{-1}. With regard to the differences in intensities and half widths, the latter two bands are assigned to spin allowed d-d transitions of Fe^{2+}, whereas the most intense band at 14870 cm^{-1} with a half width of about 5000 cm^{-1} is interpreted as an IVCT transition between Fe^{2+} and Fe^{3+} arising from about 0.05 apfu Fe^{3+} content of the synthetic scorzalite sample (Schmid-Beurmann et al. 1999). A weak band at 22890 cm^{-1} arises from a spin-forbidden d-d transition to the ($^4A_1$, ^4E_g) states of Fe^{3+} (Amthauer and Rossman 1984).

The first series of cluster molecular-orbital-(MO-)calculations on scorzalite investigates the dependence of the available spectroscopic data on the cluster size. As a complete refined geometrical structure of scorzalite itself is not yet available, these calculations are based on the fractional coordinates of lazulite (Giuseppetti and Tadini 1983) combined with the recently determined lattice parameters of scorzalite (Schmid-Beurmann et al. 1999). The local environment of Fe^{2+} corresponds approximately to a trigonally elongated octahedron so that the following analysis conveniently uses the trigonal representation of the d-orbitals:

$$t_{2g}^0 = |z^2\rangle \tag{8}$$

$$t_{2g}^{\pm} = \sqrt{\frac{2}{3}}|\delta^{\pm}\rangle \mp \sqrt{\frac{1}{2}}|\pi^{\pm}\rangle \tag{9}$$

$$e_g^{\pm} = \sqrt{\frac{1}{3}}|\delta^{\pm}\rangle \pm \sqrt{\frac{2}{3}}|\pi^{\pm}\rangle \tag{10}$$

with $|\delta^+\rangle = |x^2 - y^2\rangle$, $|\delta^-\rangle = |xy\rangle$, $|\pi^+\rangle = |xz\rangle$ and $|\pi^-\rangle = |yz\rangle$. In a trigonally elongated octahedral environment, the t_{2g}-like orbitals split according to ligand field theory in such a way that the degenerate $t_{2g}^{\pm}$-doublet is below the t_{2g}^0-orbital. From the MO-calculation, this splitting pattern is also obtained for the two smallest clusters FeO_6^{10-} and $Fe(OH)_6^{4-}$, respectively, comprising just the first coordination sphere of Fe^{2+}. The spin-down $t_{2g}^{\pm}$-orbitals are slightly split by 16 and 42 meV, respectively, whereas the t_{2g}^0-orbital is about 95 meV higher in energy. The occupied spin-down Fe(3d)-orbital exhibits predominantly d_{x2-y2}-character with some admixture of d_{xz}, d_{yz} and d_{xy}. Consequently, the calculated

TABLE 2. Calculated d-d excitation energies in cm^{-1} and quadrupole splittings ΔE_Q (in mm/s with η in brackets) for scorzalite clusters of various size

Atoms	t^{+}_{2g}*	t^{-}_{2g}*	e^{+}_{g}	e^{-}_{g}	ΔE_Q (η)
7	129	726	8259	10066	+2.73(0.79)
13	339	807	9106	10856	+3.33(0.09)
21	629	911	10429	12348	–4.15(0.42)
45	113	589	9380	13405	+3.12(0.36)
51	234	508	10195	12445	+3.76(0.44)
67	387	702	10380	12937	+3.84(0.56)
87	581	1000	10485	13526	+3.67(0.77)
95	419	863	10921	13131	–3.90(0.42)
105	395	952	10276	13010	–3.81(0.44)
117	427	976	10147	12816	–3.77(0.37)
129	436	968	10324	12687	–3.80(0.29)
139	419	976	10243	12776	–3.77(0.31)
147	387	920	10380	13058	–3.84(0.47)
95B	403	928	8038	11192	–3.88(0.61)
95C	597	1170	11006	14716	–3.71(0.82)
95D	581	1008	8920	11606	–3.81(0.66)
Exp	–	–	10490	12120	–3.99(0.6)

* Ordering for clusters with negative quadrupole splitting; for those with positive quadrupole splitting the ordering is t^{-}_{2g}, t^{0}_{2g}.

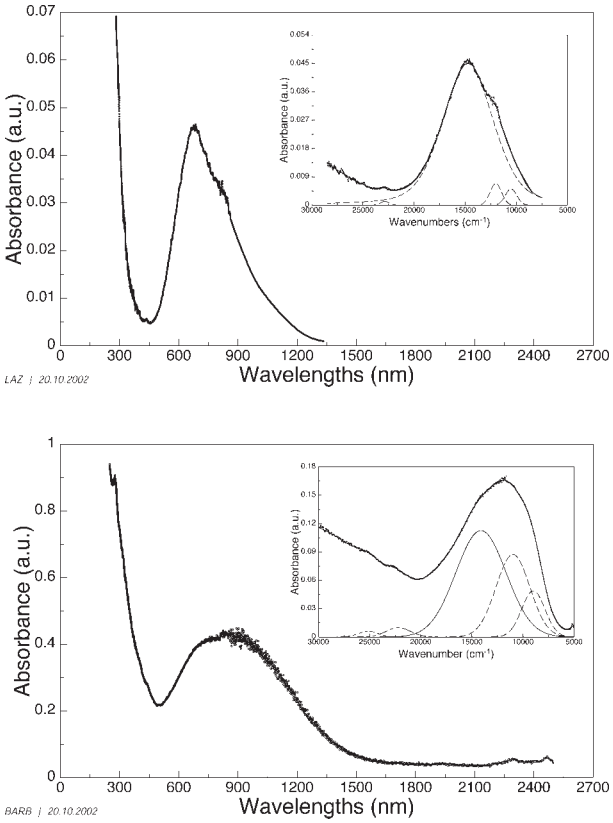

FIGURE 3. Diffuse reflectance spectra of (**a**) scorzalite and (**b**) barbosalite. The resolution into the intervalence charge transfer (IVCT) band (full line) and the two spin-allowed d-d transitions broken line) is displayed in the insert.

quadrupole splitting is positive in both cases with 2.73 mm/s (η = 0.79) and 3.33 mm/s (η = 0.09), respectively (cf., Table 2).

Adding next the two face-sharing Al-octahedra with the terminal oxygen atom replaced by fluorine in order to keep the total cluster charge small, yields a completely different picture for the resulting 21 atom-containing cluster $[Fe(OH)_6(AlF_3)_2]^{4-}$. The quadrupole splitting is now negative with –4.15 mm/s (η = 0.42) — in almost quantitative agreement with experiment, and the t^{0}_{2g}-orbital becomes the occupied spin-down Fe(3d)-orbital. Hence, it is the positive ligand field of the two Al atoms that stabilizes the t^{0}_{2g} relative to the $t^{\pm}_{2g}$ orbitals. However, further increasing the cluster size reveals this result as fortuitous, namely, adding the four phosphate tetrahedra bounded to the oxygen atoms of the first coordination sphere, again reverses the sign of the quadrupole splitting. Expanding the cluster up to 87 atoms does not change the situation, although the increase of the asymmetry parameter from 0.36 to 0.77 (Table 2) indicates a tendency that the direction of the efg will change. This happens, actually, for the cluster with 95 atoms and the composition $FeAl_2O_8(OH)_4$-$P_4O_6(OH)_6$-$P_6Al_6O_8Mg_4F_{30}$. This cluster provides the proper description of the environment of the central Fe within a sphere of 5.25 Å in the sense that all cations are included up to this distance and that all anions are correctly represented as oxygen atoms. This finding resembles the results of recent calculations on fayalite where the correct environment of Fe within a sphere of 5.2 Å was required to obtain the proper orientation of the efg (Lottermoser et al. 2002). Increasing the cluster size stepwise up to 147 atoms does not lead to any appreciable change in the d-d-excitation energies and the efg (Table 2) so that a cluster of 95 atoms appears to be size convergent with respect to the calculated spectroscopic data. Moreover, whereas the 95 atom cluster is highly compact in the sense that within a sphere of 6.42 Å only four non-hydrogen atoms have been omitted, this compactness is lost for the larger clusters. Finally, because the exact structural data of scorzalite itself are not known, additional calculations have been carried out for comparison: (1) by combining the fractional coordinates of lazulite (Giuseppetti and Tadini 1983) with the lattice parameters of barbosalite (Redhammer et al. 2000), denoted as cluster 95B in Table 2; (2) by combining the lattice parameters of scorzalite (Schmid-Beurmann et al. 1999) with the fractional coordinates of barbosalite (cluster 95C); and (3) by the structural data of barbosalite itself (cluster 95D). Although the quadrupole splitting shows only minor variations, the asymmetry parameter and the d-d-excitation energies vary considerably so that a conclusive comparison between the measured and calculated spectroscopic data is somewhat limited under this aspect.

Despite these uncertainties, the theoretical results are in satisfactory agreement with the available experimental data. The quadrupole splitting of –3.90 mm/s for the 95 atom cluster (assuming a nuclear quadrupole moment of 0.16 barn for Fe) is close to the measured value of –3.99 mm/s at 4.2 K, and the two largest calculated d-d excitation energies in the range from 10147 cm^{-1} to 10921 cm^{-1} and from 12687 cm^{-1} to 13131 cm^{-1}, respectively, (Table 2) compare well with the two measured absorption peaks at 10490 cm^{-1} and 12120 cm^{-1} (Fig. 3a), having in mind that d-d excitation energies are usually overestimated by about 10–20% in the LSDA. The measured asymmetry parameter $\eta = 0.6 \pm 0.2$ is somewhat larger than the calculated one, but is still in the range of η-values as a function of cluster size and structural variations displayed in Table 2.

Decomposition of the efg into its various contributions as

described above shows that the efg arises almost exclusively from the 3d-shell anisotropy Δn_d (–3.86 mm/s) while the other contributions are nearly negligible, viz., –0.10 mm/s arising from the 4p-shell anisotropy, –0.09 mm/s from the covalence, and +0.15 mm/s from the ligand contribution. Moreover, within the 3d-shell, neither the spin-up electrons ($\Delta n_d = 0.008$) nor the covalent admixtures of the four formally empty spin-down orbitals ($\Delta n_d = -0.022$) contribute significantly so that the 3d-shell anisotropy is virtually identical with the (negative of the) occupation number of the occupied spin-down t_{2g}^0-orbital. Accordingly, the large quadrupole splitting does not necessarily indicate very ionic Fe-O bonds. To the contrary, the average value 0.205e of the Fe-O overlap population is even larger than that of the A-site in vivianite (average value = 0.186e; Grodzicki and Amthauer 2000) that exhibits a quadrupole splitting of only 2.59 mm/s.

The temperature dependence of the efg can be simulated easily, provided that this dependence arises predominantly from thermal population of the low-lying unoccupied molecular orbitals. The thermal occupation of these orbitals at temperature T can be related to the corresponding orbital energy differences $\delta\varepsilon$ according to $\exp(-\delta\varepsilon/k_BT)$ with the Boltzmann constant k_B. As can be seen from the fourth column of Table 3, the relatively small splitting between the highest occupied and the lowest unoccupied molecular orbitals in the range between 387 and 436 cm^{-1}, obtained for clusters with at least 95 atoms (second column in Table 2), yields a pronounced calculated temperature dependence of the quadrupole splitting in quantitative agreement with the corresponding measurements on lazulite and scorzalite (second and third column of Table 3).

Results and discussion II: Barbosalite

The diffuse reflectance spectrum of barbosalite is characterized by an absorption edge at 36360 cm^{-1} and a broad asymmetric band between 5000 and 20000 cm^{-1} (Fig. 3b). As with scorzalite, the best results are obtained assuming three Gaussian-shaped absorption lines centered at 14110 cm^{-1}, 10980 cm^{-1}, and 8985 cm^{-1}. Again, the latter two bands are assigned to spin allowed d-d transitions of Fe^{2+}, whereas the most intense band at 14110 cm^{-1} with a half width of more than 3000 cm^{-1} arises from the IVCT transition between Fe^{2+} and Fe^{3+}. These values for barbosalite are somewhat smaller than those for scorzalite and the lazulite with 0.19 Fe apfu content (Amthauer and Rossman 1984) because the Fe octahedra in barbosalite are slightly expanded. These changes are also apparent in the calculations yielding a reduction of about 1500 cm^{-1} for the highest d-d transition energy in going from the scorzalite to the barbosalite structure (clusters 95 and 95D, respectively, in Table 2). Two weak bands at 22517 cm^{-1} and 25075 cm^{-1} arise from spin-forbidden Fe^{3+} d-d transitions.

Table 3. Temperature dependence of the quadrupole splitting ΔE_Q (in mm/s) for Fe^{2+} in lazulite (laz), scorzalite (sco), and barbosalite (bar)

T(K)	laz(exp)*	sco(exp)	sco(cal)†	bar(exp)‡	bar(cal)†
4.2–80	(–)4.04(1)	–3.99(2)†	–3.90	–3.798(15)	–3.81
150	–	–	–3.80	–3.748(15)	–3.79
200	–	–3.63(2)†	–3.62	(–)3.689(1)	–3.73
295–300	(–)3.32(1)	(–)3.22(1)§	–3.21	(–)3.513(1)	–3.45
400	(–)2.95(1)	–	–2.69	–	–3.05

* Amthauer and Rossman 1984.
† This work.
‡ Redhammer et al. 2000.
§ Schmid-Beurmann et al. 1999.

The cluster MO-calculations for barbosalite are based on the recently refined structural data (Redhammer et al. 2000) and are restricted to the 95 atom cluster as the most compact model for the environment of the Fe^{2+}. In the first step, the mode of spin coupling between Fe^{2+} and Fe^{3+} within the trioctahedral subunit has been determined as weakly antiferromagnetic with a coupling constant $J = -18$ cm^{-1}. However, for the following reasons, this result cannot be considered as conclusive. First, SCC-Xα generally favors antiferromagnetic (*af*) coupling compared with a ferromagnetic (*fm*) one (Antony et al. 1997). Second, for the antiferromagnetic case the calculation yields a small admixture of the lowest empty (minority spin) d-orbital of Fe^{3+} to the highest occupied (majority spin) d-orbital of Fe^{2+} which is not present in the case of the ferromagnetic spin alignment. Third, removing this admixture by replacing Fe^{2+} with Mg, yields hyperfine parameters for Fe^{3+} that are almost identical with the ferromagnetic case. Altogether, it cannot be excluded that this admixture may be an artifact of the calculation. For this reason, the spectroscopic data have been calculated for both spin arrangements. The d-d transition energies are obtained as 9180 cm^{-1} and 11840 cm^{-1} (*af*), and as 8824 cm^{-1} and 11477 cm^{-1} (*fm*), both pairs of energies being close to the measured ones. The energy of the IVCT transition with respect to the ferromagnetic spin arrangement can be derived alternatively from the total energy difference between the ground state and the excited state, where the spin-down d-electron is transferred from the Fe^{2+} to the Fe^{3+}, or from the orbital energy difference of a transition state calculation where only one half of the spin-down d-electron is transferred to the lowest spin-down d-orbital of the Fe^{3+}. The first procedure yields an IVCT energy of 14100 cm^{-1}, in perfect agreement with the experimental value of 14110 cm^{-1}, whereas the result of the transition-state calculation, displayed in Figure 4, is only insignificantly larger at 14324 cm^{-1}.

The (relativistic) electronic charge densities at the Fe nuclei are calculated as 15072.58 a_o^{-3} at Fe^{3+} and as 15069.78 a_o^{-3} at Fe^{2+} for the *fm* spin arrangement. The resulting charge-density difference of 2.80 a_o^{-3} is predominantly due to the change in the 3s density with 2.62 a_o^{-3} whereas the other contributions are about an order-of-magnitude smaller, viz., 0.46 a_o^{-3} (4s), –0.45 a_o^{-3} (2s), and 0.17 a_o^{-3} (1s). Assuming a calibration constant of –0.25 a_o^3 mm/s, the calculated isomer shift difference between the Fe^{2+} and the Fe^{3+} is 0.70 mm/s (0.59 mm/s for the *af* spin arrangement) close to the measured 0.66 mm/s at 80 K (Redhammer et al. 2000). The calculated ferrous and ferric quadrupole splittings are –3.79 mm/s (η= 0.87) and –0.58 mm/s (η= 0.99), respectively, for the antiferromagnetic and –3.81 mm/s (η= 0.90) and +0.37 mm/s (η= 0.75), respectively, for the ferromagnetic case. These results are again in excellent agreement with the experimental values of –3.798 mm/s and 0.273 mm/s (sign not determined) measured at T = 80 K (Redhammer et al. 2000). Decomposing the efg into its valence, covalence and ligand contributions yields results for the Fe^{2+} that are almost identical with those in scorzalite whereas

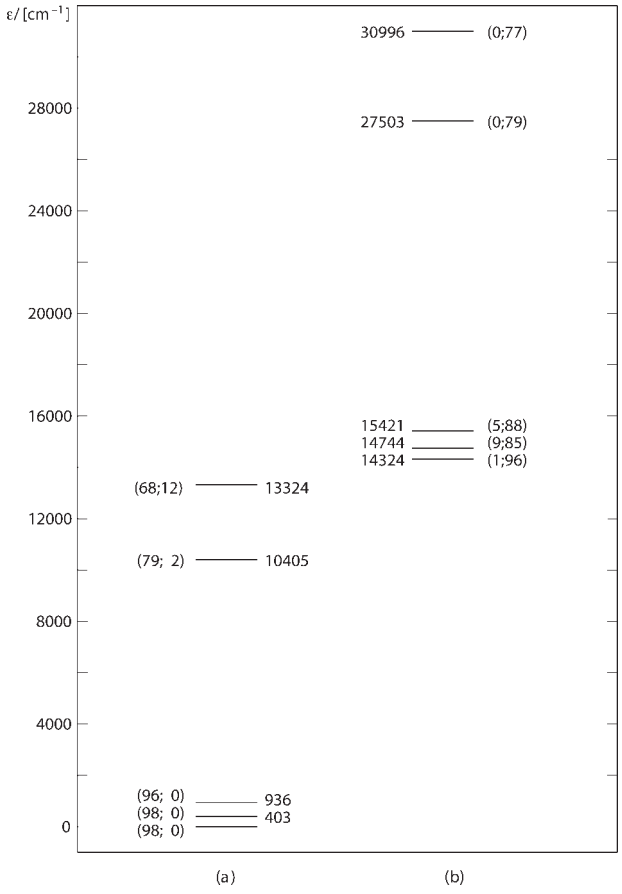

FIGURE 4. Energy diagram for the spin-down 3d molecular orbitals of (**a**) Fe^{2+} and (**b**) Fe^{3+} in barbosalite as obtained from the transition-state calculation. The lowest d-orbital at each site contains one half of an electron, and the orbital energy difference of 14324 cm^{-1} corresponds to the IVCT energy. The numbers in brackets denote the Fe(3d) percentage contribution of Fe^{2+} (first number) and Fe^{3+} (second number) to the respective molecular orbital.

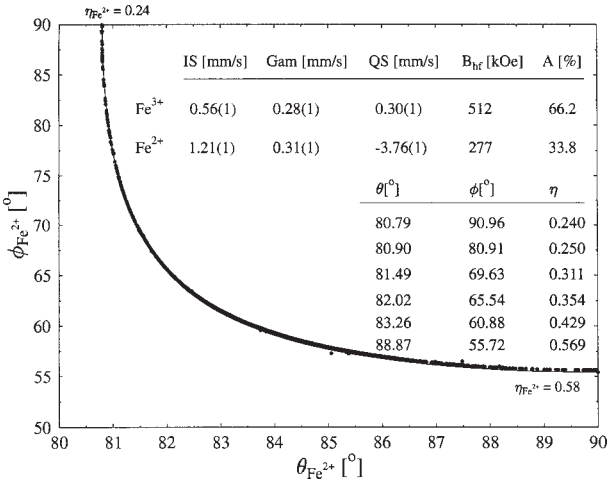

FIGURE 5. Variation of the asymmetry parameter η as a function of the angles (θ,φ) between the efg and the internal magnetic field for the ferrous site in barbosalite.

for Fe^{3+}, the valence contribution is smallest (+0.01 mm/s), as expected according to ligand field theory, but now the covalence contribution (+0.24 mm/s) is twice as large as the efg arising from the ligands (+0.12 mm/s). Hence, even in this case of a nearly spherical Fe(3d)-shell a point-charge approximation for the efg does not give the correct picture.

Altogether, the only significant deviation between measured and calculated spectroscopic data occurs in the asymmetry parameter η derived as 0.25 for the Fe^{2+} site from the low-temperature magnetic spectrum (Redhammer et al. 2000). In particular, compared with scorzalite, the measured η for barbosalite is smaller whereas the calculated η for barbosalite is larger indicating a more distorted environment of the Fe^{2+} site. Such an increased distortion is also reflected in the larger splitting of the spin-down t_{2g}-manifold that amounts to 613 cm^{-1} and 1024 cm^{-1} with respect to the t_{2g}^0-orbital. Accordingly, the calculated temperature dependence of the quadrupole splitting is less pronounced than in scorzalite (last column of Table 3) in agreement with the experimental results also given in Table 3. This apparent discrepancy between the experimentally derived η and the degree of distortion can be removed by taking into account that, in a powder spectrum without external field, the asymmetry parameter η and the angles θ and φ between the efg and the internal magnetic field are not independent of each other (Mattievich et al. 1979). From the correlation diagram between these three parameters, displayed in Figure 5, it can be seen that the combination (θ,φ) = (88°, 55.°5) yields an η-value of 0.59 that is virtually identical with the measured η in scorzalite and is much closer to the calculated η for barbosalite.

With regard to the thermodynamic properties, an examination of the bonding modes of Fe will be instructive. The calculated effective charges for Fe of +0.60 (Fe^{2+}) and +0.99 (Fe^{3+}), as well as those for the oxygen atoms between –0.35 and –0.44 exhibit substantial deviations from the formal oxidation states of +2, +3, and –2, respectively, and indicate considerable covalent character. The occupation of the valence shells of iron, viz., $Fe^{2+}(4s^{0.63}\ 4p^{0.53}\ 3d^{6.24})$ and $Fe^{3+}(4s^{0.70}\ 4p^{0.75}\ 3d^{5.56})$, reveal, however, that this covalent character is mainly due to the 4s- and 4p-electrons whereas the 3d-shell occupation numbers are only moderately increased. Correspondingly, the 3d spin densities of 3.72 (Fe^{2+}) and 4.36 (Fe^{3+}) are not too far from the free-ion values of 4 and 5, respectively. In addition, the decomposition of the Fe-O overlap populations into the contributions from the 4s–, 4p–, 3d↑ – and 3d↓–orbitals reveals that the covalent part of the Fe-O bonds is almost exclusively determined by the 4s- and 4p-electrons (Table 4). The 3d↑-electrons yield a small antibonding (negative) contribution corresponding to the fact that both the bonding and the antibonding spin-up linear combinations of the Fe(3d↑)- and the O(2p↑)-orbitals are occupied. Accordingly, the effective contribution of the 3d-electrons to the bond is at least an order of magnitude smaller compared with the 4s,4p-electrons, and the stronger covalency of the Fe^{3+}-O bonds arises solely from the smaller Fe^{3+}-O distances. Analogous results have been obtained for iron in chlorite (Lougear et al. 2000), vivianite

TABLE 4. Decomposition of the overlap population of the iron oxygen bonds in barbosalite

	d(Å)	Total	4s + 4p	3d↑	3d↓
Fe^{2+}-O_3	2.068	0.231	0.220	–0.019	0.030
Fe^{2+}-O_5	2.149	0.172	0.167	–0.016	0.021
Fe^{2+}-O_H	2.123	0.175	0.166	–0.018	0.027
Fe^{3+}-O_1	1.934	0.335	0.296	–0.027	0.066
Fe^{3+}-$O_{3,5}$*	2.056	0.221	0.208	–0.027	0.040
Fe^{3+}-O_H*	2.073	0.204	0.184	–0.024	0.044

* Averaged values.

(Grodzicki and Amthauer 2000), and epidote (Grodzicki et al. 2001). Consequently, although the covalent contribution may constitute a relatively small part of the total Fe-O bond energy, these results suggest that, e.g., a discussion of ligand-field stabilization energies solely in terms of the d electrons requires careful justification.

Finally, the isotropic magnetic coupling constant J between two adjacent Fe^{3+}-octahedra within a chain has been determined. Employing a cluster with 158 atoms, modelling the surrounding of a ferric double octahedron, an antiferromagnetic coupling of –84.6 cm^{-1} or 122 K is obtained which is rather strong for a pair of hydroxo-bridged Fe^{3+}s. Although the calculated coupling constant for an isolated pair of Fe^{3+}-octahedra cannot directly be compared with the measured Neel temperature between 160 K and 173 K (Redhammer et al. 2000), it is in the correct order of magnitude and thus appears reasonable.

ACKNOWLEDGMENTS

This research is funded by the Austrian Fonds zur Förderung der wissenschaftlichen Forschung (FWF), grant number P12424-GEO. All calculations have been carried out at the Research Institute of Software Technology (RIST) of the TechnoZ in Salzburg. G.J.R. acknowledges the financial support by an FWF grant via an APART scholarship.

REFERENCES CITED

Akai, H., Blügel, S., Zeller, R., and Dederichs, P.H. (1986) Isomer shifts and their relation to charge transfer in dilute Fe alloys. Physical Review Letters, 56, 2407–2410.

Amthauer, G. and Rossman, G.R. (1984) Mixed valence of iron in minerals with cation clusters. Physics and Chemistry of Minerals, 11, 37–51

Antony, J., Grodzicki, M., and Trautwein, A.X. (1997) Local Density Functional Study of Oxo-iron(IV) Porphyrin Complexes and their One-electron Oxidized Derivatives. Axial Ligand Effects. Journal of Physical Chemistry, A101, 2692–2701.

Blaha, P., Schwarz, K., Faber, W., and Luitz, J. (2000) Calculations of electric field gradients in solids: How theory can complement experiment. Hyperfine Interactions, 126, 389–395.

Dufek, P., Blaha, P., and Schwarz, K. (1995) Determination of the nuclear quadrupole moment of ^{57}Fe. Physical Review Letters, 75, 3545–3548

Duff, K.J. (1974) Calibration of the isomer shifts for ^{57}Fe. Physical Review, B9, 66–72.

Eriksson, O. and Svane, A. (1989) Isomer shifts and hyperfine fields in iron compounds. Journal of Physics Condensed Matter, 1, 1589–1599.

Giuseppetti, G. and Tadini, C. (1983) Lazulite, $(Mg,Fe)Al_2(OH)_2(PO_4)_2$: structure refinement and hydrogen bonding. Neues Jahrbuch Mineralogie Monatshefte, 1983(9), 410–416.

Grodzicki, M. (1980) A self-consistent-charge Xα method I. Theory. Journal of Physics, B13, 2683–2691.

———(1985) Theorie und Anwendungen der Self-Consistent-Charge-Xα Methode; Thesis of habilitation, Hamburg 1985.

Grodzicki, M. and Amthauer, G. (2000) Electronic and magnetic structure of vivianite: cluster molecular orbital calculations. Physics and Chemistry of Minerals, 27, 694–702.

Grodzicki, M., Männing, V., Trautwein, A.X., and Friedt, J.M. (1987) Calibration of isomer shifts and quadrupole coupling constants for ^{119}Sn, ^{127}I and ^{129}I as derived from SCC-Xα calculations and Mössbauer measurements. Journal of Physics, B20, 5595–5625.

Grodzicki, M., Heuss-Assbichler, S., and Amthauer, G. (2001) Mössbauer investigations and molecular orbital calculations on epidote. Physics and Chemistry of Minerals, 28, 675–681.

Hush, N.S. (1967) Intervalence-transfer absorption 2. Theoretical considerations and spectroscopic data. Progress in Inorganic Chemistry, 8, 391–612.

Jansen, N., Spiering, H., Gütlich, P., Stahl, D., Kniep, R., Eyert, V., Kübler, J., and Schmidt, P.C. (1992) Mössbauer-Spektroskopie und Elektronenstrukturberechnungen an Nitridoferraten(III): $Li_3[FeN_2]$ und $Ba_3[FeN_3]$. Angewandte Chemie, 104, 1632–1634.

Keutel, H., Käpplinger, I., Jäger, E.G., Grodzicki, M., Schünemann, V., and Trautwein, A.X. (1999) Structural, magnetic and electronic properties of a pentacoordinated intermediate-spin (S = 3/2) iron(III) complex with a macrocyclic $[N_4]^{2-}$ ligand. Inorganic Chemistry, 38, 2320–2327.

Kortüm, G. and Oelkrug, D. (1966) Reflexionsspektren fester Stoffe. Naturwissenschaften, 23, 600–609.

Kubelka, P. and Munk, F. (1931) Ein Beitrag zur Optik der Farbanstriche. Zeitschrift für technische Physik, 12, 5593–5601.

Lauer, S., Marathe, V.R., and Trautwein, A.X. (1979) Sternheimer shielding using various approximations. Physical Review, A19, 1852–1861.

Lindberg, M.L. and Christ, C.L. (1959) Crystal structures of the isostructural minerals lazulite, scorzalite and barbosalite. Acta Crystallographica 12, 695–697.

Lottermoser, W., Steiner, K., Grodzicki, M., Jiang, K., Scharfetter, G., Bats, J.W., Redhammer, G., Treutmann, W., Hosoya, S., and Amthauer, G. (2002) The electric field gradient in synthetic fayalite α-Fe_2SiO_4 at moderate temperatures. Physics and Chemistry of Minerals, 29, 112–121.

Lougear, A., Grodzicki, M., Bertoldi, C., Trautwein, A.X., Steiner, K., and Amthauer, G. (2000) Mössbauer and molecular orbital study of chlorites. Physics and Chemistry of Minerals, 27, 258–269.

Mattievich, E., Vugman, N.V., Diehl, L.M.A., and Danon, J. (1979) Analytical interpretation of temperature dependent combined quadrupolar and magnetic hyperfine interaction in $Fe^{2+}Fe^{3+}{}_2(PO_4)_2(OH)_2$ (barbosalite). Journal de Physique, 40, 1195–1198.

Millet, J.M.M., Rouzies, D., and Vedrine, J.C. (1995) Isobutyric acid oxidative dehydrogenation over iron hydroxyphosphates. II.Tentative description of the catalytic sites based on Mössbauer spectroscopic study. Applied Catalysis, A124, 205–219.

Nieuwpoort, W.C., Post, D., and van Duijnen, P.T. (1978) Calibration constant for ^{57}Fe Mössbauer isomer shifts derived from ab initio self-consistent-field calculations on octahedral FeF_6 and $Fe(CN)_6$ clusters. Physical Review, B17, 91–98.

Noodleman, L. (1981) Valence bond description of antiferromagnetic coupling in transition metal dimers. Journal of Chemical Physics, 74, 5737–5743.

Paulsen, H., Ding, X.Q., Grodzicki, M., Butzlaff, C., Trautwein, A.X., Hartung, R., and Wieghardt, K. (1994) Spectroscopic and theoretical studies on a three-iron cluster with linear arrangement. Chemical Physics, 184, 149–162.

Ray, S.N. and Das, T.P. (1977) Nuclear quadrupole interaction in the Fe^{2+} ion including many-body effects. Physical Review, B16, 4794–4804.

Redhammer, G.J., Tippelt, G., Roth, G., Lottermoser, W., and Amthauer, G. (2000) Structure and Mössbauer spectroscopy of barbosalite $Fe^{2+}Fe^{3+}{}_2(PO_4)_2(OH)_2$ between 80 K and 300 K. Physics and Chemistry of Minerals, 27, 419–429

Rouzies, D. and Millet, J.M.M. (1993) Mössbauer spectroscopic study of synthetic lipscombite and barbosalite at room temperature. Hyperfine Interactions, 77, 11–18.

Schmid-Beurmann, P., Knitter, S., and Cemic, L. (1999) Crystal chemical properties of synthetic lazulite-scorzalite solid-solution series. Physics and Chemistry of Minerals, 26, 496–505.

Schünemann, V. and Winkler, H. (2000) Structure and dynamics of biomolecules studied by Mössbauer spectroscopy. Reports on Progress in Physics, 63, 263–353.

Sieber, N.H., Tillmanns, E., and Hofmeister, W. (1987) Structure of hentschelite, $CuFe_2(PO_4)_2(OH)_2$, a new member of the lazulite group. Acta Crystallographica, C43, 1855–1857.

Slater, J.C. (1974) Quantum theory of molecules and solids, vol. 4. McGraw-Hill, New York.

Van der Heyden, M., Micklitz, H., Bukshpan, S., and Longouche, G. (1987) Systematics in the ionization states of ^{57}Fe following the electron capture decay of ^{57}Co in different rare-gas matrices. Physical Review, B36, 38–43.

Zhang, Q., Zhang, Y., and Wang, D. (1987) Isomer shift calibration of Fe nucleus by self-consistent all-electron LAPW band calculation. Communications in Theoretical Physics, 8, 139–151.

MANUSCRIPT RECEIVED MARCH 5, 2002
MANUSCRIPT ACCEPTED DECEMBER 13, 2002
MANUSCRIPT HANDLED BY M. DARBY DYAR